2011

Study of a Magnetic Filter System for the Characterization of Particle Magnetic Property

Lin Li
Washington University in St. Louis

Paul S. Greenberg
Microgravity Combustion and Reacting Systems Branch, NASA-Glenn Research Center, Cleveland, Ohio, USA

Kenneth W. Street Jr.
Microgravity Combustion and Reacting Systems Branch, NASA-Glenn Research Center, Cleveland, Ohio, USA

Da-Ren Chen
Washington University in St. Louis, chen@me.wustl.edu

Aerosol Science and Technology, 45:327–335, 2011

ISSN: 0278-6826 print / 1521-7388 online
DOI: 10.1080/02786826.2010.534514

Study of a Magnetic Filter System for the Characterization of Particle Magnetic Property

Lin Li,[1] Paul S. Greenberg,[2] Kenneth W. Street, Jr.,[2] and Da-Ren Chen[1]

[1]*Department of Energy, Environmental and Chemical Engineering, Washington University in St. Louis, St. Louis, Missouri, USA*

[2]*Microgravity Combustion and Reacting Systems Branch, NASA-Glenn Research Center, Cleveland, Ohio, USA*

A magnetic filter system has been constructed, and its performance has been investigated, to measure the magnetic property of monodisperse γ-Fe_2O_3 particles in the size range from 100 to 300 nm. In the system, SS 430 screens are placed in the magnetic filter element and exposed to a strong external magnetic field generated by an electric coil. The high magnetic field gradient resulted from magnetized fine wires enhances the collection of magnetic particles in addition to the particle collection via the diffusion mechanism. The particle concentrations at the upstream and downstream of the magnetic filter element were measured by an Ultrafine Condensation Particle Counter (UCPC, TSI model 3025A). Particle penetration obtained in the experiment is a function of particle size, particle magnetic property, and wire magnetization. To retrieve the magnetic property of characterized particles from the measured penetration data, a numerical model was further developed using the finite element package COMSOL Multiphysics 3.5. In this modeling, a single mesh screen is assumed to be represented by unit cells. The flow, the magnetic fields, and particle trajectory were solved in a unit cell. The relationship between particle penetration and magnetic property can then be obtained via this model for the given particle size, aerosol flowrate, and external magnetic field strength. The numerical model was first validated by comparing the experimental penetration with the simulation results for the case of 100, 150, and 250 nm γ-Fe_2O_3 particles having the magnetic susceptibility characterized by Vibrating Sample Magnetometer (VSM). The magnetic susceptibilities of other sizes from 100 to 300 nm were then derived from this model according to the measured penetration data.

1. INTRODUCTION

Magnetic particles are of great interest in fundamental research and industrial applications. They are used in a wide range of applications in catalysis (Noronha et al. 1997), magnetocooling (Roy et al. 1993), recording devices (Prinz 1998), purification of enzymes and other biotical substances (Airapetyan et al. 2001), as well as water purification devices (Kobe et al. 2001). Many medical applications need submicron- and nanometer-sized magnetic particles (Häfeli et al. 1999) for drug delivery via biocompatible magnetic substances, cell separation, hyperthermia, cancer therapy, and aneurysm treatment, to name just a few examples. Fine particles can also display different forms of magnetism: ferromagnetism, ferrimagnetism, paramagnetism, diamagnetism, and superparamagnetism, distinguished by the influence of the external magnetic field on their magnetic moment, which also depends on the raw material and the generation conditions. Additionally, in the size range from submicrometer down to nanometer, the magnetic properties change very strongly with particle diameter. One of the main characteristics of magnetic particles is their magnetic moment. Hence, the determination of the particles' magnetic moment is an important problem of interest to both scientific and engineering efforts.

The vibrating sample magnetometer (VSM) is a widely used instrument for determining the magnetic properties of a large variety of materials since its invention by Foner (1959). The superconducting quantum interference device (SQUID) can be configured as a magnetometer to detect extremely small magnetic fields from magnetic particles (Clarke 1994). Recently, the magnetic moment per unit mass of magnetic nanoparticles was found by using an atomic force microscope (AFM) (Park et al. 2008). All these method are used for off-line analysis, which means it takes significant time to collect sufficient samples before the measurements can be performed.

An absolute on-line magnetic moment measurement of iron particles, synthesized by aerosol methods ranging in size from 40 to 170 nm, was introduced by Kauffeldt et al. (1996). This method uses a set of Ni screens in the form of wire mesh to establish a high-gradient magnetic field for removing nanometer-sized magnetic particles from their carry gas stream. The high-gradient magnetic separation (HGMS) is in fact widely used

Received 21 June 2010; accepted 13 October 2010.

The authors (Li and Chen) are grateful for the financial support provided by the NASA Glen Research Center (Grant No. NNX07AN27G).

Address correspondence to Da-Ren Chen, Department of Energy, Environmental and Chemical Engineering, Washington University in St. Louis, Campus Box 1180, One Brookings Drive, St. Louis, MO 63130, USA. E-mail: chen@me.wustl.edu

in the treatment of biological fluids, of industrial fluids, and of wastewater (Rembaum et al. 1982; Miltenyi et al. 1990; Moeser et al. 2002; Bucak et al. 2003; Chen et al. 2007a; Anand 1985; Shaikh and Dixit 1992; Nedelcu and Watson 2002; Newns and Pascoe 2002; Karapinar 2003). Significant effort has been made to model the performance of magnetic filters since the introduction of HGMS. To simplify the geometrical complexity in magnetic filtration systems, the particle trajectory models, which calculate the influence of various forces on the interaction between a single particle and a single wire collector, have been used to predict the effect of key design factors on the capture cross section for a clean magnetic filter (Watson 1973; Lawson et al. 1977; Gerber and Birss 1983; Ying et al. 2000; Ebner and Ritter 2001; Chen et al. 2007b). Particle trajectory models were developed to retrieve the magnetic moment of particles from the measured penetration difference between the case that applied an external magnetic field and the case that did not (Kauffeldt et al. 1996; Zarutskaya and Shapiro 2000). These models made two assumptions: (1) it was assumed that the particle magnetic moment is independent of the external magnetic field applied; (2) the combined effect of the Brownian motion and particle rotation on the particle capture efficiency did not exceed more than a few percent. Accordingly, in modeling the magnetically assisted capture, the particles may be effectively assumed to be diffusionless and to have their magnetic moment vectors oriented along the local magnetic field. However, these models have not been experimentally validated prior to their use. Because the actual magnetic property of the testing particles used in the experiment was not characterized by other reference methods (for example, VSM or AFM), nor was it compared with the property obtained via the models themselves. Further, these models did not consider the effect of flow and magnetic field variation due to the presence of adjacent wires, although in reality the magnetic filter is constructed by well-defined mesh screens.

In this study, a magnetic filter consisting of ten SS 430 screens with 200 mesh was designed and tested using monodisperse γ-Fe_2O_3 particles ranging in size from 100 to 300 nm at different flow rates. To obtain the particles' magnetic susceptibility, we developed a particle trajectory model to describe the behavior and collection of magnetic particles from carry gas in the magnetic filter. To validate the proposed model, we compared the magnetic susceptibility of particles obtained from the proposed model to that obtained from VSM. Further, the effects of filtration operation conditions and particle diameters on their behavior and magnetic capture efficiency were numerically investigated.

2. DESIGN AND EVALUATION OF MAGNETIC FILTER SYSTEM

Figure 1 shows the schematic diagram of the studied magnetic filter system, in which a set of parallel screens were used as the filtration element, similar to that used in a screen-type diffusion battery (Cheng and Yeh 1980). The metal mesh screens were made of SS 430 magnetic wires. The carrier gas loaded with magnetic particles flowed through the filter element in the direction perpendicular to the screens. The screens were then magnetized by an external magnetic field, also in the direction perpendicular to the screens. The external magnetic field was generated by an electric coil wound around the case of the filter element holder. With the system configuration, the deposition of particles in the magnetic filter element is governed by the magnetic force experienced by particles when moving nearby the magnetized wires of the screens. The magnetic force experienced by particles is, in general, a function of the particle size, particle magnetic property, and wire magnetization.

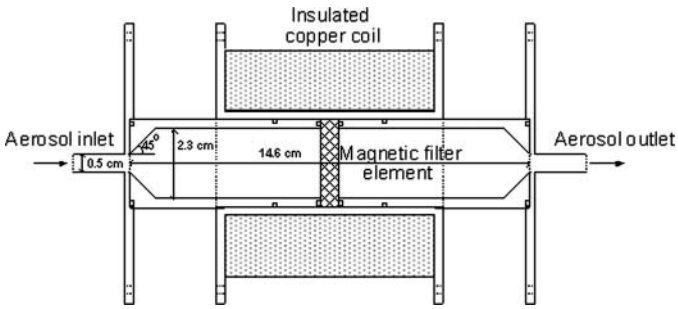

FIG. 1. Schematic diagram of the studied magnetic filter system.

Figure 2 shows the experimental setup for the penetration measurement of the magnetic filter element. Magnetic γ-Fe_2O_3 particles (Sigma-Aldrich 544884) were aerosolized with a home-made Collison atomizer (Liu and Piu 1974). The output flow rate from the atomizer was 4.0 lpm at $2.07*10^5$ Pa for inlet air pressure. Droplets produced by the atomizer were passed first through a Po^{210} radioactive neutralizer to minimize the electrical charges on the particles, and then through a diffusion dryer with silicone gel as the desiccant to remove the solvent in the droplets.

A differential mobility analyzer (DMA, TSI Model 3081) was used in the downstream of the above-described polydisperse aerosol generation system to classify monodisperse particles ranging in size from 100 to 300 nm. A Kr^{85} radioactive particle charger was used to place a well-defined charge distribution on polydisperse particles prior to the introduction of the DMA. The DMA was operated at an aerosol flowrate of 1.5 lpm and a sheath flowrate of 10.0 lpm. Since the particles exiting from the DMA are electrically charged, a Po^{210} neutralizer and an electrostatic precipitator were utilized at the DMA exit to obtain electrically neutral particles for testing. The total flowrate through the magnetic filter element was controlled by both the pump of an Ultrafine Condensation Particle Counter (UCPC, TSI model 3025A), operated at a flow rate of 1.5 lpm, and a separate vacuum pump with a needle valve to adjust the desired flowrate. The aerosol stream from the three way valve to the UCPC was equally separated into two pathways: one with the magnetic filter and one without. The tubing length of each

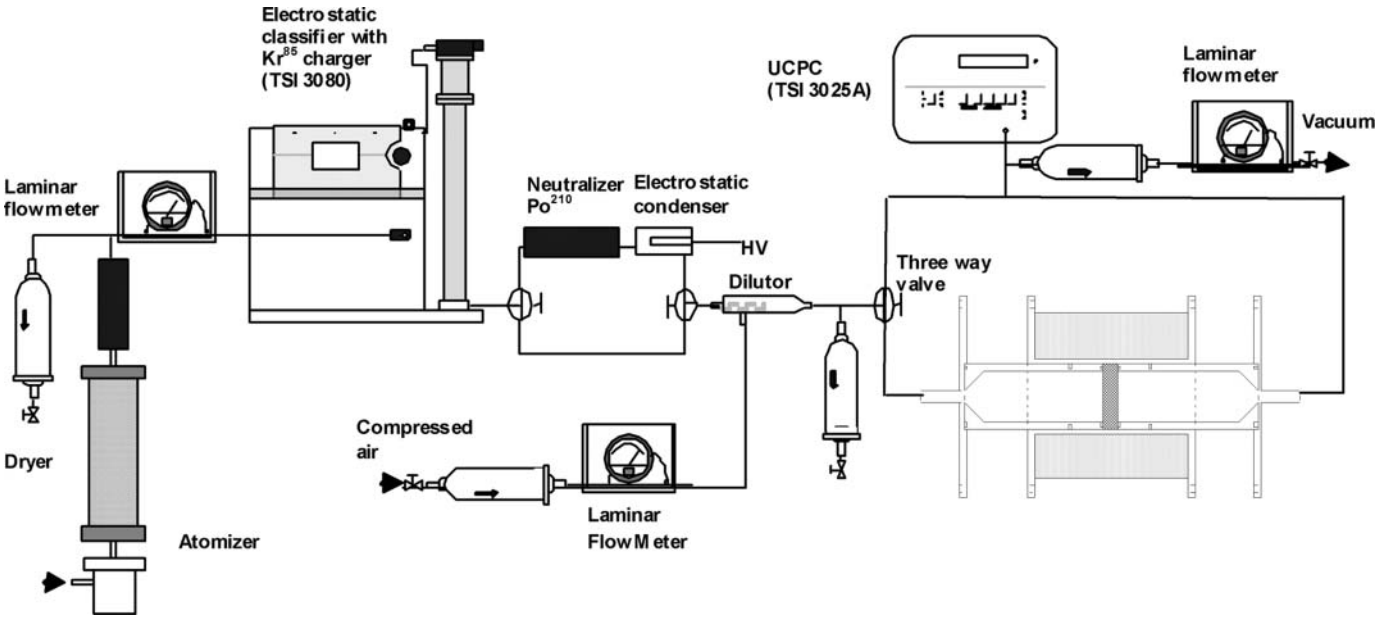

FIG. 2. Schematic diagram of the experimental setup for the evaluation of magnetic filter system.

pathway was about 20 cm. The particle number concentrations up- and down-stream of the magnetic filter were measured by UCPC. The particle penetration P through the magnetic filter with the element was then obtained by a ratio of the particle downstream concentration N_{dn} to the upstream one N_{up}:

$$Penetration = \frac{N_{dn}}{N_{up}}. \quad [1]$$

Note that, in our experiment, the upstream concentrations of monodisperse test particles were kept on the order of $10^3 \sim 10^4$ #/cm^3. Particle coagulation can thus be neglected during the transportation. The transmission efficiency of the filter holder (i.e., no filter element installed), defined as the ratio of down- and up-stream concentrations, was also measured and the values at different sizes were about 98% or higher. The particle transport loss in the duct wall is also negligible in the prototype.

3. MODELING OF MAGNETIC FILTER ELEMENT

The measured penetration P through the studied magnetic filter element, which is a function of particle size, particle magnetic property, and wire magnetization, could be predicted by calculating the fate of individual particles, and hence the capture of particles in the magnetic filter element. To determine the particle fate in the filter element, the flow and magnetic fields must be first calculated.

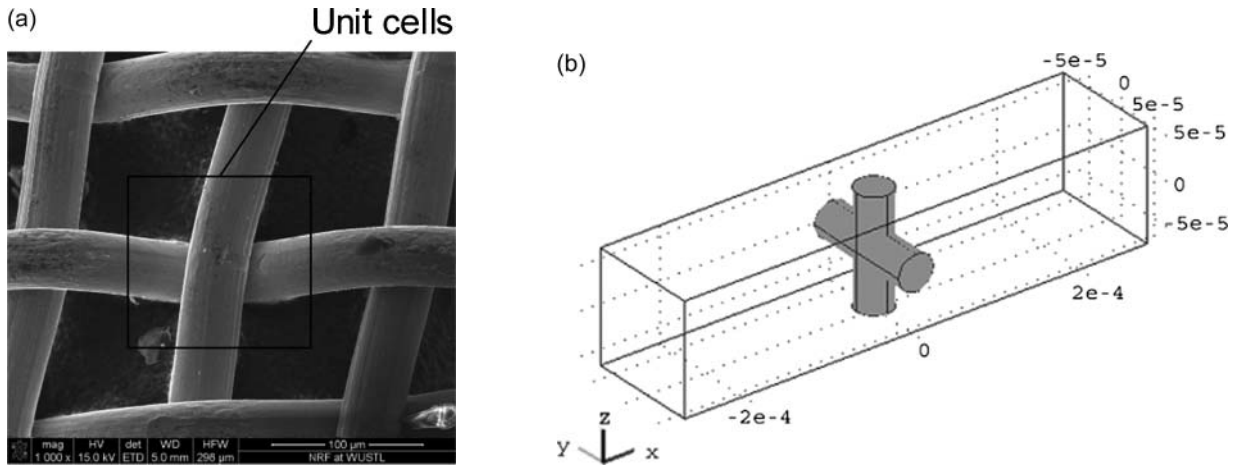

FIG. 3. (a) Unit cells as the basic elements for a single mesh screen; (b) the computational domain for a unit cell.

3.1. Calculation of Flow and Magnetic Fields

The finite element package COMSOL Multiphysics 3.5 was used to numerically solve the flow and magnetic fields in the magnetic filter element. To reduce the geometrical complexity of the filter element, we assume that a single metal screen can be represented by the replica of unit cells, as shown in Figure 3. According to the SEM micrograph, the wire diameter and spacing for the single 200 mesh SS 430 screen are about 40.5 and 86.5 μm, respectively. A wire cross with the diameter D_w of 41 μm was used in a standard cell. Since the spacing between the two adjacent mesh screens in the filter element was set at 0.5 mm, the volume of the unit cell was set at 130*130*550 μm^3.

The flow field in the unit cell was calculated by solving the continuity and 3D Navier-Stokes equations with the assumption of incompressible fluid having density ρ and viscosity η:

$$\nabla \cdot \vec{u} = 0 \quad [2]$$

$$\rho[\frac{\partial \vec{u}}{\partial t} + (\nabla \vec{u}) \cdot \vec{u}] = -\nabla P + \eta \nabla^2 \vec{u}. \quad [3]$$

The inlet flow velocity was assumed constant, uniform and equal to the face velocity $\vec{u}_\infty$ of the filter element, entering the cell in the x-direction. No slip boundary condition was applied at the wire surface. Symmetric boundary conditions were applied to the surrounding boundaries due to the replica of unit cells. A typical example of the calculated flow field in a unit cell is given in Figure 4a.

The magnetic force upon magnetic particles was determined by evaluating the magnetic field $\vec{H}$ in the unit cell. To calculate the magnetic field in a unit cell, the computational domain was divided into two regions with very distinct magnetic behaviors. One is the non-magnetizable region, which is unoccupied by the wires, and the other is the magnetized region occupied by the wires. The Maxwell equations for conservative magnetic fields were used within these two regions:

$$\nabla^2 \varphi_i = 0 \quad [4]$$

$$\nabla^2 \varphi_e = 0, \quad [5]$$

where φ_i and φ_e are the scalar magnetic potentials for wire-occupied and non-magnetizable regions, respectively, and are related to the magnetic field strengths $\vec{H}_i$ and $\vec{H}_e$ according to

$$\vec{H}_i = -\nabla \varphi_i \quad [6]$$

$$\vec{H}_e = -\nabla \varphi_e. \quad [7]$$

Considering the demagnetization factor, when the applied magnetic field $\vec{H}_0$ measured by AlphaLab DC magnetometer is perpendicular to the wire principle axis, the internal magnetic field $\vec{H}_i$ could be expressed as (Watson 1978):

$$\vec{H}_i = \vec{H}_0 - \vec{M}_f/2\mu_0, \quad [8]$$

where μ_0 is the magnetic permeability of free space. The magnetic induction $\vec{B}$ is then expressed as

$$\vec{B}_i = \mu_0(\vec{H}_i + \vec{M}_f), \quad [9]$$

where $\vec{M}_f$ is the wire magnetization measured by VSM as a function of the external magnetic field. In our study the wire magnetization are 83.6 and 160.8 kA/m at the external magnetic field of 20 and 40 kA/m, respectively.

At the wire surface, the continuities of magnetic potentials (i.e., φ_i and φ_e) and normal magnetic fluxes (i.e., $\vec{B}_i$ and $\vec{B}_e$) in wire-occupied and un-magnetizable regions were applied. The symmetric boundary condition was applied to the surrounding boundary due to cell replication. Figure 4b shows a typical example of the normal magnetic field in a unit cell.

3.2. Calculation of Individual Particle Trajectories

Particle penetration through a unit cell can be calculated by indentifying the limiting trajectory of approaching particles, which can be divided into those that end by colliding on the wire cross surface and those that simply pass the wire cross surface. The above modeling idea is illustrated in Figure 5a.

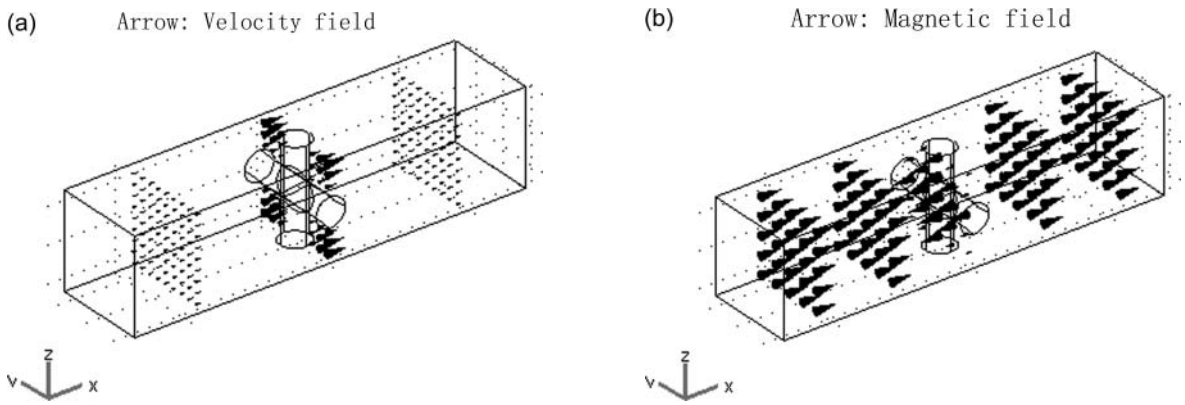

FIG. 4. (a) Flow field in the unit cell at the aerosol flowrate of 0.06 m/s; (b) Magnetic field in the unit at the external magnetic field strength of 20,000 A/m.

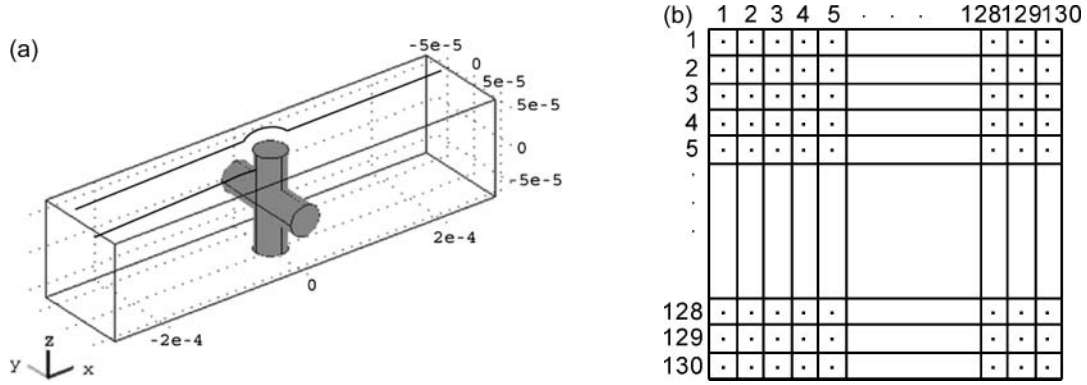

FIG. 5. (a) Illustration of limiting particle trajectory idea for particle penetration calculation; (b) the particle release profile at the cell entrance.

The following assumptions were used to calculate of individual particle trajectory:

1. According to the previous study of Zarutskaya and Shapiro (2000), particles are spherical in shape, and their rotational effects are negligible. Particles' magnetic susceptibility is assumed to be constant, and their magnetic moments are assumed to be oriented in the direction of the magnetic field.
2. Under a low Reynolds number flow system, the particle trajectory can be calculated by the force balance equation, including gravitational ($\vec{F}_g$), magnetic ($\vec{F}_m$), drag ($\vec{F}_d$), and random ($\vec{F}_{br}$) forces.
3. No particle re-entrainment occurs, and deposited particles do not significantly alter the flow and magnetic fields in the unit cell.

The trajectory of a submicron particle moving in a gas with velocity $\vec{v}$ under the action of gravitational, magnetic, drag, and random forces is determined by the force balance equations based on the Newton's second law.

$$m_p \frac{d\vec{v}}{dt} = \vec{F}_d + \vec{F}_g + \vec{F}_m + \vec{F}_{br} \qquad [10]$$

Particle drag force $\vec{F}_d$ is expressed as

$$\vec{F}_d = f(\vec{u} - \vec{v}). \qquad [11]$$

Here, m_p is the particle mass; t the time variable; $\vec{u}$ the flow velocity vector; and f the particle friction coefficient given by the Stokes law as $f = 3\pi\mu d_p/C$ (Friedlander 2000), where C is the Cunningham slip correction factor, expressed as

$$C = 1 + \frac{2\lambda}{d_p}\left(1.142 + 0.558 \times \exp\left(-\frac{0.999 d_p}{2\lambda}\right)\right), \qquad [12]$$

where λ is the mean free path.

Because of the small size of particles, the magnetic field in the particle is assumed to be approximately uniform. Further, the magnetic interaction between particles is neglected due to the low concentration of testing particles. The following expression was then used to evaluate the magnetic force $\vec{F}_m$ on a magnetic particle:

$$\vec{F}_m = \mu_0 \nabla(\vec{M} \cdot \vec{H}), \qquad [13]$$

where μ_0 is the magnetic permeability of free space, $\vec{H}$ the magnetic field strength, and $\vec{M}$ the particle magnetic moment, whose scale is related to the magnetization of particle by

$$M = \frac{\chi}{1 + \chi/3} H V_p, \qquad [14]$$

where χ is the particle magnetic susceptibility, and V_p the particle volume (O'Handley 2000).

In Brownian motion, a particle at time t and position p will make a random displacement r from its previous point with regard to time and position. The resulting distribution of r is expected to be (1) Gaussian (normal with a mean of zero and a standard deviation of one), (2) to be independent, and (3) have a root mean square displacement of $\sqrt{2Dt}$ in its x, y, and z coordinates. The random displacement r in one coordinate can be calculated as

$$r = \frac{\sqrt{2Dt}}{\sqrt{2\pi}} e^{-\frac{\xi^2}{2}}, \qquad [15]$$

where ξ is a random number.

The trajectory for a given particle was determined by solving Equation (10) using the Runge-Kutta method of the 4th order. As shown in Figure 5b, the uniform particle concentration profile was assumed at the cell entrance, which was divided into 130*130 squares. A single particle was released from the center of each square up to 100 times. The cell collection efficiency E_c is the ratio of the number of particles N captured

TABLE 1
Values and dimensions of the parameters used in the modeling

Parameters	Units	Values
Fluid density	kg m^{-3}	1.2
Fluid viscosity	kg(ms)$^{-1}$	1.81E-5
Fluid temperature	T	298
Mean fluid velocity	m/s	0.06-0.22
Screen material		SS 430
Fiber diameter	μm	41
Magnetic field strength	A/m	20000, 40000
Particle density	kg m^{-3}	5242 (γ-Fe_2O_3) 1.98 (KCl)
Particle size	nm	100∼300 (γ-Fe_2O_3) 50∼300 (KCl)

by the wire cross to the number of particles N_0 entering the cell:

$$E_c = \frac{N}{N_0} \quad [16]$$

Since cell efficiency represents the presence of a single mesh screen, the overall penetration P through n screens can then be calculated by (Brown 1993):

$$P = exp(-nE_c). \quad [17]$$

As a summary of all the modeled cases, the values and dimensions of the parameters used in our numerical study are given in Table 1.

4. MODEL VALIDATION AND ANALYSIS

To verify the numerical model, we first compared the calculated penetration with the experimental one for the case of potassium chloride, KCl, particles, in which the particle magnetic force is negligible. Figure 6 compares of the calculated and the experimental penetrations through the magnetic filter element at different carry gas flowrates for KCl particles ranging in size from 50 to 300 nm. The error bar of the experimental data represents the flow fluctuation of UCPC. Good agreement between numerical and experimental penetration data was obtained in the studied size range. For the case of 50 nm particles, the calculated penetration is slightly higher than the experimental. It may be attributed to the pre-set time step for the particle trajectory calculation. The pre-set time step for marching a particle in the unit cell may be large enough that particle collection on the wire cross may be underestimated due to the particle diffusion process.

Prior to the validation of our numerical model, we measured the magnetic susceptibility of 100, 150, and 250 nm γ-Fe_2O_3 particles by VSM. Monodisperse γ-Fe_2O_3 particles classified by the DMA (TSI model 3081) were collected using an electrostatic precipitator. Figure 7 shows the TEM image of 150 nm γ-Fe_2O_3

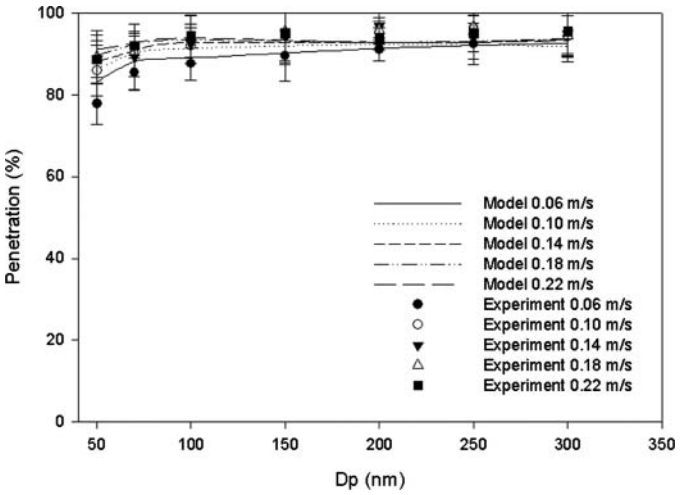

FIG. 6. Comparison of calculated and experimental penetration through the magnetic filter element at different flowartes for KCl particles in the size range from 50 nm to 300 nm.

particles. The classified particles are nearly spherical in shape. Collected particles were then filled in a small sealed glass tube for the VSM characterization. Figure 8 shows the magnetization curves of 100, 150, and 250 nm γ-Fe_2O_3 particles obtained by VSM. The magnetic susceptibility is defined as the slope of the initial magnetization curve as a function of magnetic field strength.

To verify our numerical model including magnetic force we compared numerical penetration with experimental data through

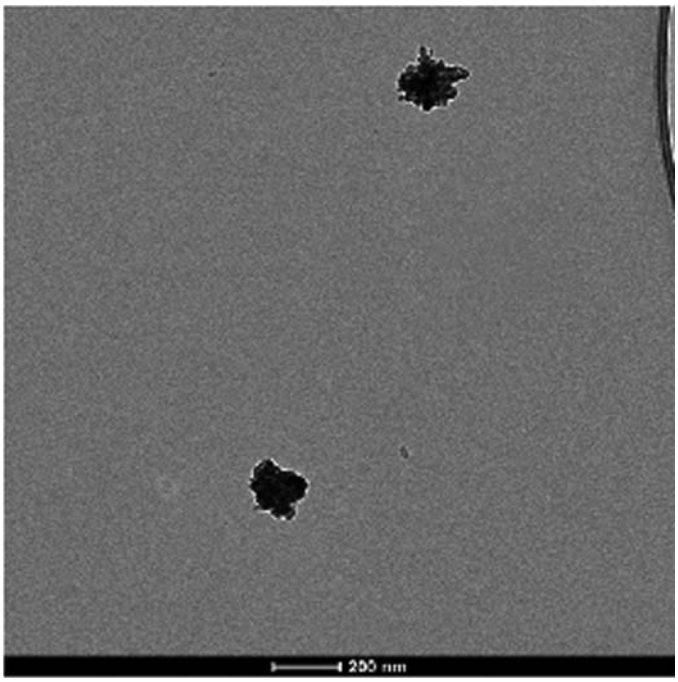

FIG. 7. TEM image of 150 nm γ-Fe_2O_3 particles.

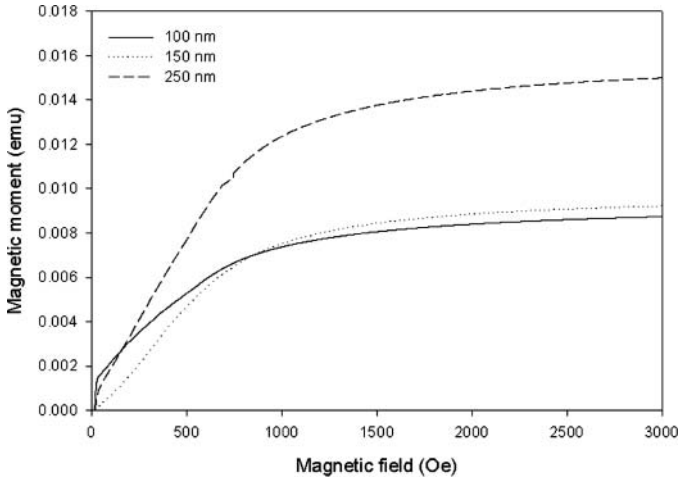

FIG. 8. Magnetization curves of 100, 150, and 250 nm γ-Fe_2O_3 particles characterized by VSM.

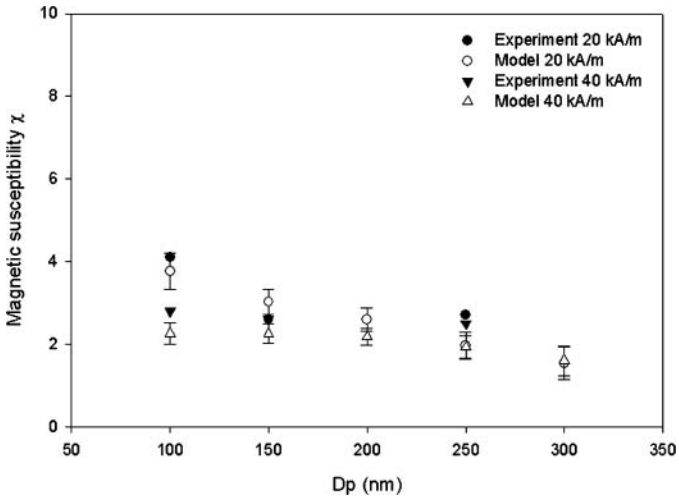

FIG. 10. Derived magnetic susceptibility of γ-Fe_2O_3 particles in the size range from 100 to 300 nm at the external magnetic fields of both 20 and 40 kA/m.

the magnetic filter element at different flowrates for 100, 150, and 250 nm γ-Fe_2O_3 particles for the estimated external magnetic fields of both 20 and 40 kA/m (Figure 9). The numerical penetration was calculated using the proposed model base on the measured magnetic susceptibility data by VSM. We found that particle penetration increases with an increase in aerosol flow velocity, and decreases with an increase in external magnetic field strength and particle size. The good agreement between the calculated and the experimental penetrations validates our numerical model. In general, the discrepancy between the experimental and the calculated penetration is less than 10%.

With this model, the particle penetration curves through the magnetic filter element as a function of magnetic susceptibility were first calculated for γ-Fe_2O_3 particles in size ranging from 100 to 300 nm at different flowrates and in the external magnetic fields of 20 and 40 kA/m. From the above-calculated curves, the correlated particle magnetic susceptibility was then retrieved from the measured particle penetration data. The derived magnetic susceptibility of studied γ-Fe_2O_3 particles as a function of particle size is shown in Figure 10. For comparison, the magnetic susceptibility data of 100, 150, and 250 nm γ-Fe_2O_3 particles measured by VSM were also included in the figure. Based on the calculated curve, the error bar of the given magnetic susceptibility data was determined from that of the penetration data taking into account of the UCPC flow fluctuation. Generally, the derived magnetic susceptibility of γ-Fe_2O_3 particles is in the same order of magnitude. However, a slight difference between the external magnetic field of 20 kA/m and the external magnetic field

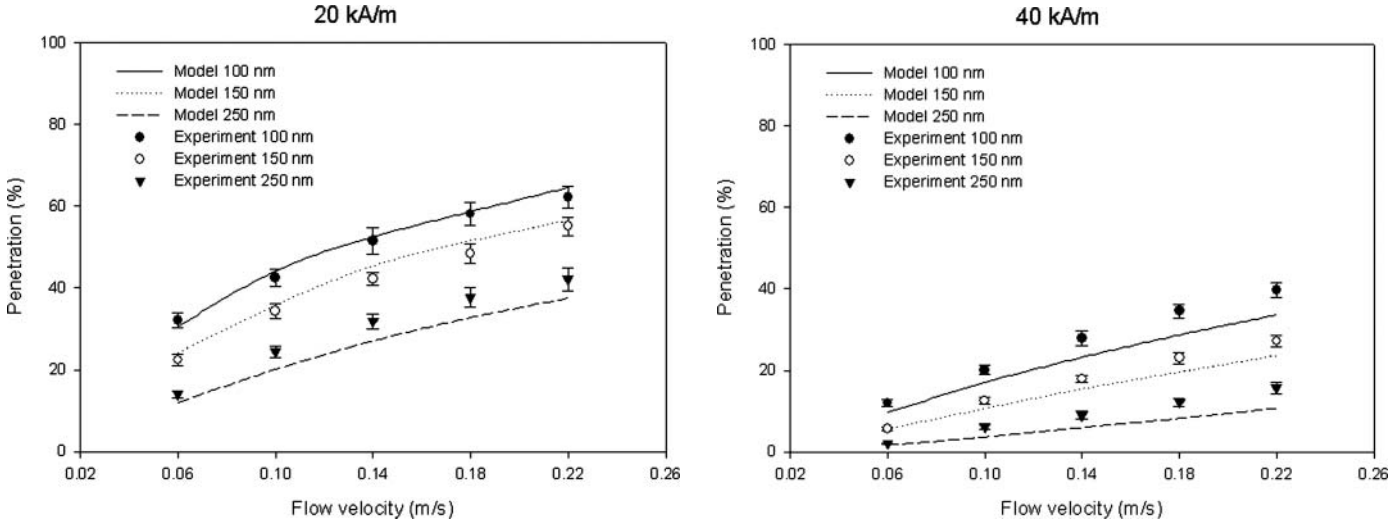

FIG. 9. Comparison of calculated and experimental penetration through the magnetic filter element at estimated 20 and 40 kA/m external magnetic field and different flow rates for 100, 150, and 250 nm γ-Fe_2O_3 particles.

40 kA/m were observed, especially in the smaller particle sizes. Note that the particle magnetic susceptibility χ was assumed constant in our model even though particles may experience different magnetic field strengths in the particle trajectory calculation. For ferrimagnetic materials, the theoretical relationship between magnetization and magnetic field strength is not linear (as the magnetization curve shown in Figure 8 for 100 nm γ-Fe_2O_3 particles), indicating that magnetic susceptibility is a function of magnetic field strength. It may be why a small deviation is observed between the two different magnetic field strengths.

A gradual decrease of the magnetic susceptibility of studied γ-Fe_2O_3 particles with increasing particle size is also observed in Figure 10, which shows that particle magnetic susceptibility has a minor dependence on size. But the variation of magnetic susceptibility for γ-Fe_2O_3 particles in general remains small in the studied size range.

5. CONCLUSION

A magnetic filter system has been constructed and its performance has been evaluated to measure particles' magnetic property by using monodisperse γ-Fe_2O_3 particles ranging in size from 100 to 300 nm. In the system, SS 430 screens were placed in the magnetic filter element and exposed to an external magnetic field generated by an electric coil. Under the exposure of an external magnetic field, mesh screens were then magnetized and the high magnetic field gradient created by magnetized wires facilitated the collection of magnetic particles when they were passed through the filter element. The particle concentrations at the upstream and the downstream of the magnetic filter element were measured by an UCPC. Particle penetration obtained in the experiment was found to be a function of particle size, particle magnetic property and wire magnetization in general. In this study, a numerical model was also developed via the finite element package COMSOL Multiphysics 3.5. In the modeling, a single mesh screen is represented by an assembly of unit cells. The model then solved the flow, the magnetic fields, and the particle trajectory in a representative unit cell. The relationship between the particle penetration and the magnetic property for a given particle size, aerosol flowrate, and external magnetic field was obtained by the model. The numerical model was validated by comparing the calculated penetration with the experimental data, the former being calculated with the measured magnetic susceptibility of 100, 150, and 250 nm γ-Fe_2O_3 particles via VSM. The magnetic susceptibilities of other sizes from 100 to 300 nm were also obtained by this model, according to the measured penetration data. In general, the magnetic susceptibility of γ-Fe_2O_3 particles is in the same order of magnitude. We observed that particle magnetic susceptibility has a minor dependence on the particle size and applied external magnetic field strength. The lowest detection limit of particle magnetic susceptibility for our magnetic filter system is on the order of 10^{-4} based on the model calculation. For particles with magnetic susceptibility lower than 10^{-4}, the resultant magnetic force is so small that it could not enhance the particle trapping in the filter element when compared with the trapping by diffusion. Note that the lower detection limits of the studied system can be further extended by optimizing the filter system by, for example, using the higher external magnetic field strength, using mesh screens with stronger magnetic property and finer meshes, and so on. This optimization happens because the magnetic force experienced by magnetic particles is also a function of external magnetic field strength and magnetic field gradient.

REFERENCES

Airapetyan, S. S., Balayan, G. G., and Khachatryan, A. G. (2001). Synthesis and Some Characteristics of Magnetic Matrices for Fixation of Biologically Active Substances. *Russian J. Appl. Chem*. 74(3):519–521.

Anand, P., Etzel, J. E., and Friedlaender, F. J. (1985). Heavy Metals Removal by High Gradient Magnetic Separation. *IEEE Trans. on Magn*. 21(5):2062–2064.

Brown, R. C. (1993). *Air Filtration*. Pergamon Press. London.

Bucak, S., Jones, D. A., Laibinis, P. E., and Hatton, T. A. (2003). Protein Separations Using Colloidal Magnetic Nanoparticles. *Biotechnol. Prog*. 19(2): 477–484.

Chen, H., Ebner, A. D., Bockenfeld, D., Ritter, J. A., Kaminski, M. D., Liu, X., Rempfer, D., and Rosengart, A. J. (2007a). A Comprehensive In Vitro Investigation of a Portable Magnetic Separator Device for Human Blood Detoxification. *Phys. Med. Biol*. 52:6053-6072.

Chen, H., Bockenfeld, D., Rempfer, D., Kaminski, M. D., and Rosengart, A. J. (2007b). Three-Dimensional Modeling of a Portable Medical Device for Magnetic Separation of Particles from Biological Fluids. *Phys. Med. Biol*. 52:5205–5218.

Cheng, Y. S., and Yeh, H. C. (1980). Theory of a Screen-Type Diffusion Battery. *J. Aerosol Sci*. 11:313–320.

Clarke. J. (1994, August). SQUIDS. *Sci. Am.* 46–53.

Ebner, A. D., and Ritter, J. A. (2001). New Correlation for the Capture Cross Section in High-Gradient Magnetic Separation. *AIChE J.* 47(2):303–313.

Foner, S. (1959). Versatile and Sensitive Vibrating-Sample Magnetometer. *Rev. Sci. Inst.* 30(7):548–557.

Friedlander, S. K. (2000). *Smoke, Dust, and Haze*. Oxford University Press, New York.

Gerber, R. and Birss, R. R. (1983). *High Gradient Magnetic Separation*. John Wiley & Sons, New York.

Häfeli, U. O., Casillas, S., Dietz, D. W., Pauer, G. J., Rybicki, L. A., Conzone, S. D., and Day, D. E. (1999). Hepatic Tumor Radioembolization in a Rat Model Using Radioactive Rhenium(^{186}Re/^{188}Re) Glass Microspheres. *Int. J. Radiat. Oncol. Biol. Phys*. 44(1):189–199.

Karapinar, N. (2003). Magnetic Separation of Ferrihydrite from Wastewater by Magnetic Seeding and High-Gradient Magnetic Separation. *Int. J. Miner. Process*. 71:45–54.

Kauffeldt, Th., Kleinwechter, H., and Schmidt-Ott, A. (1996). Absolute Online Measurement of the Magnetic Moment of Aerosol Particles. *Chem. Eng. Commun*. 151:169–185.

Kobe, S., Drazic, G., McGuiness, P. J., and Strazisar, J. (2001). The Influence of the Magnetic Field on the Crystallisation Form of Calcium Carbonate and the Testing of a Magnetic Water-Treatment Device. *J Magn. Magn. Mater*. 236:71–76.

Lawson, Jr., W. F., Simons, W. H., and Treat, R. P. (1977). The Dynamics of a Particle Attracted by a Magnetized Wire. *J. Appl. Phys*. 48:32133224.

Liu, B. Y. H., and Piu, D. Y. H. (1974). A Submicrion Aerosol Standard and the Primary, Absolute Calibration of the Condensation Nuclei Counter. *J. Colloid Interface Sci.* 47:155–171.

Miltenyi, S., Müller, W., Weichel, W., and Radbruch, A. (1990). High-Gradient Magnetic Cell-Separation with Macs. *Cytometry.* 11(2):231–2388.

Moeser, G., Roach, K. A., Green, W. H., Laibinis, P. E., and Hatton, T. A. (2002). Water-Based Magnetic Fluids as Extractants for Synthetic Organic Compounds. *Ind. Eng. Chem. Res*. 414(19):4739–4749.

Nedelcu, S., and Watson, J. H. P. (2002). Magnetic Separator with Transversally Magnetised Disk Permanent Magnets. *Miner. Eng*. 15:355–359.

Newns, A., and Pascoe, R. D. (2002). Influence of Path Length and Slurry Velocity on the Removal of Iron from Kaolin Using a High Gradient Magnetic Separator. *Miner. Eng*. 15:465–467.

Noronha, F. B., Schmal, M., Nicot, C., Moraweck, B., and Frety, R. (1997). Characterization of Graphite-Supported Palladium-Cobalt Catalysts by Temperature-Programmed Reduction and Magnetic Measurements. *J. Catalysis*. 168(1):42–50.

O'Handley R. C. (2000). *Modern Magnetic Materials: Principles and Applications*. John Wiley & Sons, New York.

Park, J. W., Yoo, I. S., Chang, W. S., Lee, E. C., Ju, H., Chung, B. H., and Kim, B. S. (2008). Magnetic Moment Measurement of Magnetic Nanoparticles Using Atomic Force Microscopy. *Measurement Sci. Technol*. 19:017005.

Prinz, G. A. (1998). Magnetoelectronics. *Science*. 282:1660–1663.

Rembaum, A., Yen, R. C. K., Kempner, D. H., and Ugelstad, J. (1982). Cell-Labeling and Magnetic Separation by Means of Immunoreagents Based on Polyacrolein Microspheres. *J. Immunol. Methods*. 52(3):341–351.

Roy, S., Das, D., Chakravorty, D., and Agrawal, D. C. (1993). Magnetic Properties of Glass-Metal Nanocomposites Prepared by the Sol-Gel Route and Hot Pressing. *J. Appl. Phys*. 74:4746–4749.

Shaikh, A. M. H., and Dixit, S. G. (1992). Removal of Phosphate from Waters by Precipitation and High Gradient Magnetic Separation. *Water Res*. 26(6):845–852.

Watson, J. H. P. (1973). Magnetic Filtration. *J. Appl. Phys*. 44:4209–4213.

Watson, J. H. P. (1978). Improvements of a Low-field, High-Intensity Matrix Separator. *IEEE Transaction on Magnetics.* 14(5):392–394.

Ying, T. -Y., Yiacoumi, S., and Tsouris, C. (2000). High-Gradient Magnetically Seeded Filtration. *Chem. Eng. Sci*. 55:1101–1113.

Zarutskaya, T., and Shapiro, M. (2000). Capture of Nanoparticles by Magnetic Filters. *J. Aerosol Sci*. 31(8):907–921.